Renewable and Sustainable Energy Reviews 76 (2017) 1053–1065

Contents lists available at ScienceDirect

Renewable and Sustainable Energy Reviews

journal homepage: www.elsevier.com/locate/rser

Influence of solar photovoltaic array on operation of grid-interactive fifteen-level modular multilevel converter with emphasis on power quality

ARTICLE INFO

Keywords:
Fuzzy
Multi-level
Solar
Harmonics
Dynamic voltage
Power quality

ABSTRACT

This paper unveils an operational impact of variable Solar Photovoltaic (SPV) array into 15-level single-stage Modular Multilevel Converter (MMC) thyristorized operated system. A MMC system is developed in which the working of three sub-system modules has been coordinated at a Point of Common Coupling (PCC). In addition, each of 15-level sub-system has been operated at a Resistance Inductance (RL) and a SPV array load. Furthermore, the investigation of DC power inversion into AC power has been elaborated by varying the switching angles of thyristors from 100° to 180°for an individual module. The operation of MMC system has been coordinated with Dynamic Voltage Restorer (DVR), where its performance has been estimated during grid faults under unity power factor conditions. Especially, the investigation on Power Quality (PQ) has been highlighted at PCC by operating with proportional integral and fuzzy logic controlled DVR. It has been verified that response with fuzzy logic DVR scheme is able to control the unbalanced conditions, under steady-state and transient conditions effectively. The effectiveness of the proposed controller is demonstrated by using standard IEEE-519/1547, which stipulates that harmonic level in utility injected current by any SPV source cannot exceed 5%. Therefore, a reduction in harmonics and DC offset is ensured satisfactorily, among all variables at PCC according to IEEE-519/1547 standard at fundamental frequency.

1. Introduction

Nowadays, the fossil fuel has been the main energy supplier for worldwide economy. This, however, has caused many environmental problems such as global warming and air pollution. Therefore, with regard to worldwide trend of green energy, the solar power technology [1,2] is envisaged to become one of the most promising type of energy resources [3]. At present, the number of Solar Photovoltaic (SPV) installations have seen an exponential growth [4], mainly due to the government and utility companies supporting green energy [5]. The deep integration of any renewable energy resource mainly depends on inexpensive technological improvement of global emissions and precise controlling techniques for Power Quality (PQ) [6,7].

The SPV systems with Pulse Width Modulation (PWM) controlled [8,9] inverters generate a square waveform with large harmonic content [10]. To overcome this, multilevel inverters offer sinusoidal waveform with reduced harmonic content and lower electromagnetic interference. As mentioned in references [11–14], the multilevel inverters exhibit lower switching frequency than standard PWM inverters thus, demonstrate the reduced switching losses. The modular type of multilevel converter has strong potential to replace cascaded type multilevel converter, especially in medium voltage applications [15]. Currently, intensive research is going in Modular Multilevel Converter (MMC) systems owing to their potential for medium power applications. MMC generates low harmonic at output voltage, thus eliminating filtering requirements. Moreover, it also allows avoiding interfacing transformer [16] thus, extending higher number of output levels easily. Although, the study of MMC systems is investigated with many applications, but this study has not been carried with single-stage SPV configuration. Therefore, this paper presents the analytic study on SPV grid-interactive power conversion system, coordinating with single-stage 15-level MMC system.

For a three-phase grid connected SPV system, a mathematical model based on a hybrid fuzzy-neural [17] and a 9-rule fuzzy logic control [18] has been proposed. It has been demonstrated that the fuzzy-neural control provides faster convergence speed and good dynamic operation around maximum power point. The control schemes implemented are proposed to regulate the DC bus voltage and reactive output power in rotating *dq*-reference frame [19–21]. The operation of a hybrid cascaded type multilevel inverter topology having three leg and H-bridge cells, has been investigated in [22]. In addition, it has been reported that maximum steps are produced in output voltage, with minimum number of required switching capacitors [23,24]. Various advantages of multilevel inverter systems which are: low power dissipation during switching, reduced harmonic distortion and electromagnetic interference; have been reported in [25]. It is their inherent ability that these inverters are capable to generate power of high quality from SPV systems and provide flexible functionality with improved PQ. The suitability of multilevel inverter for single-phase grid interaction is analyzed in [26]. The presence of several DC sources on DC side of inverter makes such inverters attractive for SPV applications.

A single-phase five-level [27], three-phase five-level [28] grid-connected SPV inverter and a multilevel H-bridge inverter [29] including battery energy storage is proposed in the literature. Total Harmonic Distortion (THD) is controlled through a digital type proportional integral current control type algorithm. This algorithm maintains the current injected into the grid sinusoidal with reduced harmonic distortion content. Additionally, the THD in voltage for a multilevel H-bridge inverter which includes battery as energy storage source, is found to be less than 6%.

http://dx.doi.org/10.1016/j.rser.2017.03.092
Received 26 July 2016; Received in revised form 12 February 2017; Accepted 20 March 2017
1364-0321/

Furthermore, to decrease the cost on account of increasing switching devices and transformers, an efficient multilevel inverter switching pattern is proposed in [30]. It is equipped with two cascaded type transformers having a series connected secondary winding. In this system, the switching losses are further reduced by implementing a hybrid PWM type control [31]. In order to divide the power among the various converter modules, the proposed design is implemented for two different systems: one for a 10 kW-1,32 kV generation and another one for a 1 MW-13.2 kV medium voltage generation system. A prototype single-phase cascaded H-bridge inverter has been built in [32], which can configure to work as 5-, 7- or 9-level inverter according to the number of activated levels. The targeted 3rd, 5th and 7th harmonic have been eliminated with non-equal DC voltage sources, using particle swarm optimization. A five-level diode clamped inverter has been connected to grid by a traditional three-phase transformer through a space vector modulation as grid interface [33]. The THD analysis has been reported for inverter output voltage-15.61%, and grid current-1.98%. A single-phase multilevel inverter configuration that conjoins three series connected full bridge inverters and a single half bridge inverter for SPV system is proposed in [34]. Theoretical calculation of power losses and THD of output voltage-9.85% without using passive filters and 3.91% with filter inductance, is reported. A three-phase single stage grid interactive inverter with adaptive fuzzy-logic type Maximum Power Point Tracking (MPPT) capability is reported in [35]. The level of THD for the inverter output current is in the limits of international standards (< 5%), and the efficiencies of MPPT algorithm and total system are measured as 98.78% and 93.12%, respectively. An experimental validation to prove low current THD factor is reported [36] by developing a single-phase cascaded multilevel inverter delivering power from two SPV strings.

This paper aims to describe the modeling and control of a SPV array supported 15-level three module in single-stage configuration. The operation of MMC is evaluated for three-phase grid interactive system during grid faults. The impact of Dynamic Voltage Restorer (DVR) [37–39] is analyzed during the faulted conditions. The operation of DVR has been controlled through Proportional Integral (PI) and Fuzzy Logic Control (FLC). Moreover, the thyristor of each MMC module is operated in continuous-current conduction mode at unity power factor. Since the SPV array is non-linear in nature [1], the real and reactive output power are derived under stochastically changing environmental conditions for three modules of MMC system. It is envisaged that reactive power requirement of Resistance Inductance Capacitance (*RLC)* load is achieved by each of three modules, and hence its compensation is achieved. In addition, the simulation of FLC-DVR is found to be satisfactory to eliminate unbalanced swell and sag for variables at Point of Common Coupling (PCC) [40]. Using Fast Fourier Transform (FFT) [41,42] technique, the calculated values of THD for load current and utility current are estimated to be 1.98% and 1.95%, respectively, which conforms the correctness of implemented proposed system according to IEEE-519/1547 standard [43].

2. Computational system model

The simulation scheme of 15-level MMC system fed SPV array is depicted in Fig. 1. A MMC system is an arrangement of three multilevel converter modules, which are connected to a three-phase electric grid at PCC through an Inductance-Capacitance-Inductance (*LCL)* filter. Each module of MMC system is operated at a Resistance Inductance-*RL* and an experimental validated SPV array. Further, the three SPV arrays are operated under different levels of solar radiation levels: 600 W/m^2, 800 W/m^2 and 1000 W/m^2, and different cell temperatures: 10 °C, 20 °C and

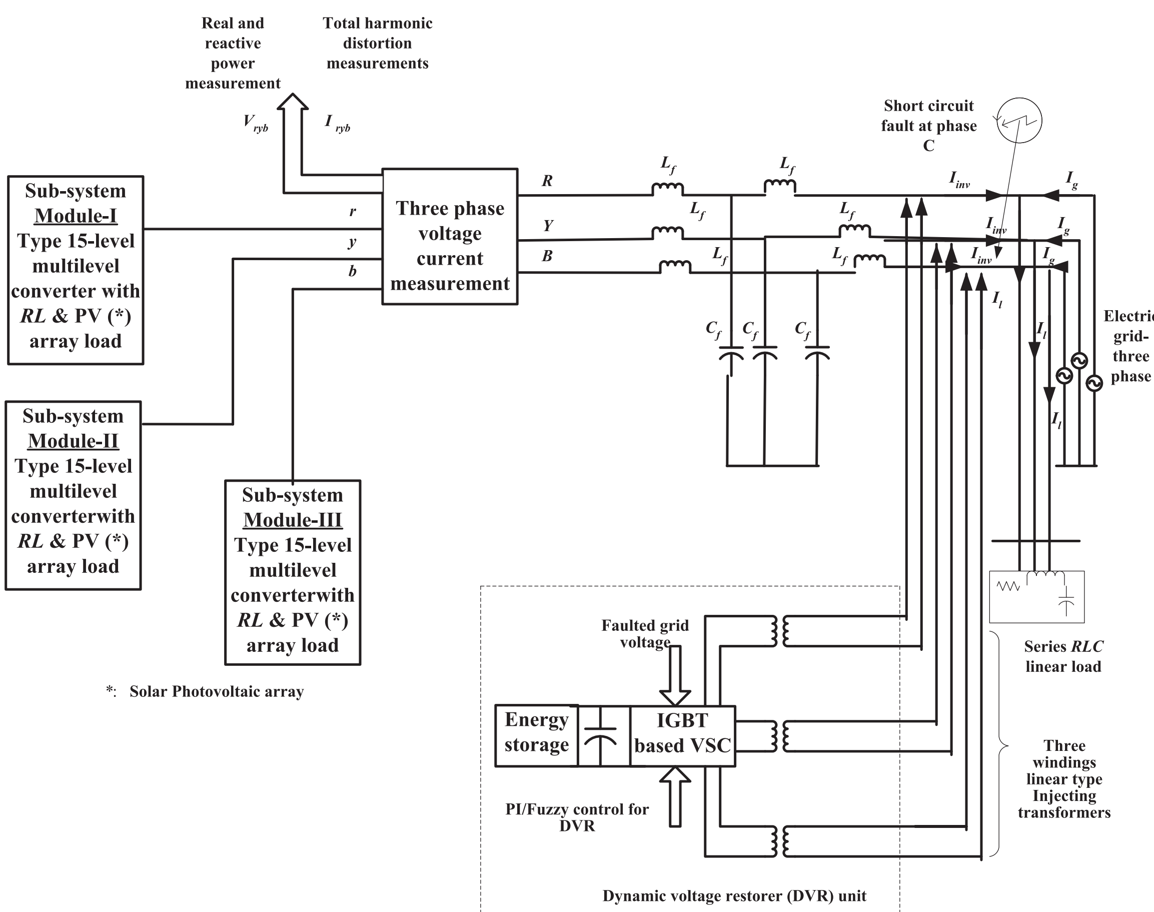

Fig. 1. Block diagram of single-stage three-phase grid-interactive 15-level MMC modules fed *RL* and SPV arrays.

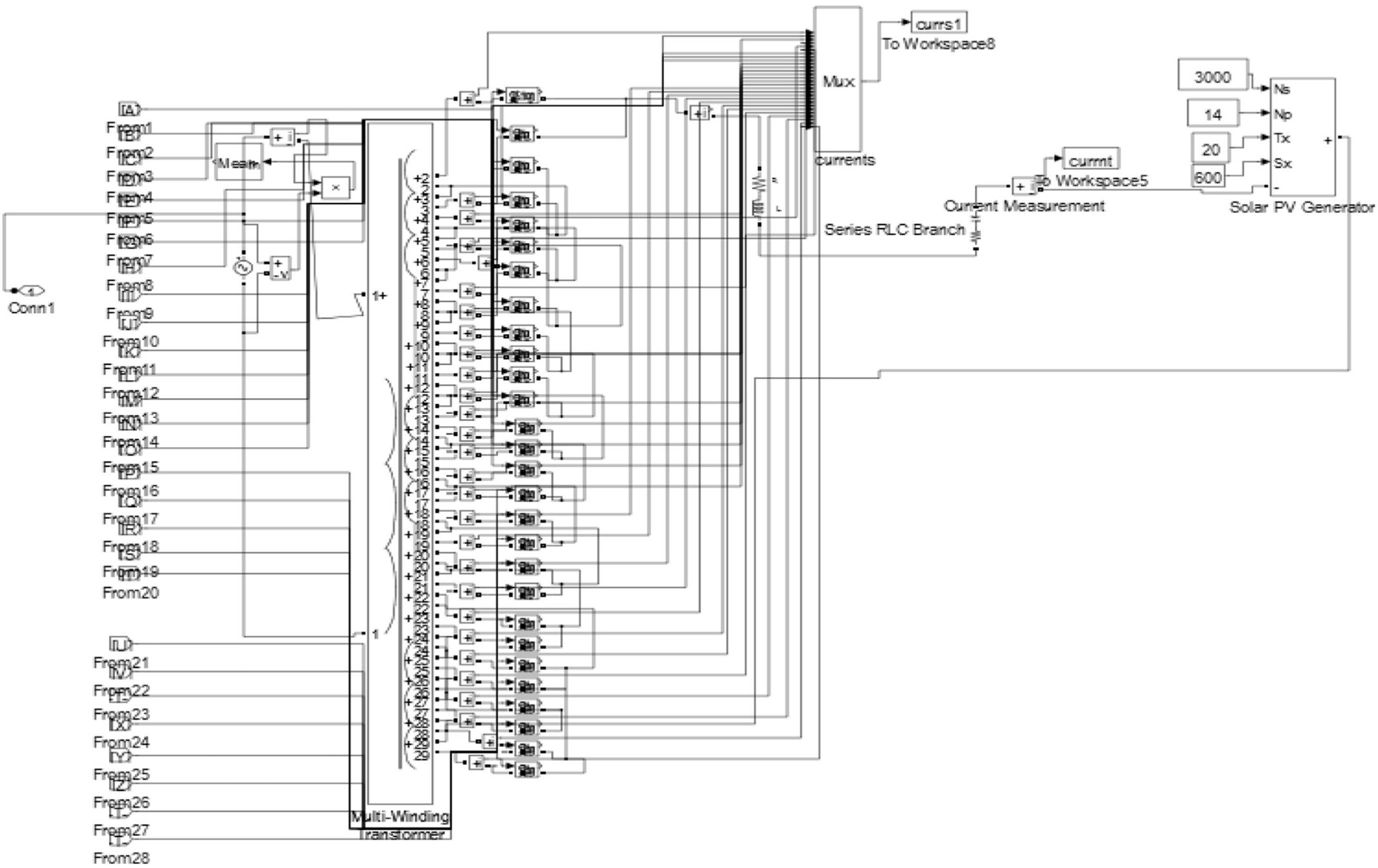

Fig. 2. Simulink model for a 15-level multilevel converter with a *RL* & a SPV array connected load.

Table 1
Phase delays of thyristors for a single module (in s).

Upper leg	0.0057	0.0067	0.0077	0.0087	0.0097	0.0107	0.0117	0.0127	0.0137	0.0147	0.0157	0.0167	0.0177	0.0187
Lower leg	0.0158	0.0168	0.0178	0.0188	0.0198	0.0208	0.0218	0.0228	0.0238	0.0248	0.0258	0.0268	0.0278	0.0288

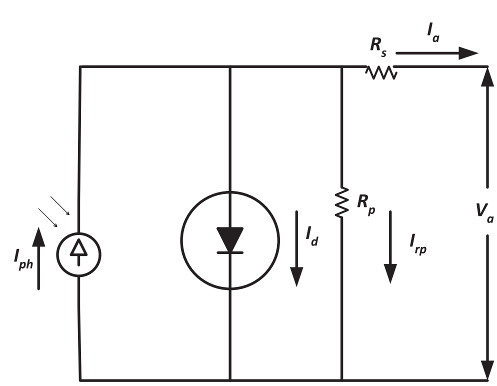

Fig. 3. Electrical equivalent of a SPV cell.

30 °C, respectively. The *LCL* filter comprising of two series inductance and a parallel capacitor, prevents the harmonics produced due to thyristors in filtrating into the utility grid. A single 15-level module of MMC system consists of 14 pairs of thyristors, which are operated in inversion mode by varying switching angle, α of each thyristor. In order to evaluate the performance at unity power factor, the proposed system is operated and tested at linear *RLC* load. A three-phase fault is introduced at phase C on the three-phase grid side. The presence of three-phase fault affects the power generated by an electric grid and a MMC system. Hence, in this paper, an attempt has been made to investigate the effect of Insulated Gate Bipolar Transistor (IGBT) based DVR in addressing concerns of important PQ issues. Furthermore, the DVR has been used in distributed system to control the flow of active power and highlighting the reactive power compensation. Additionally, DVR has the ability to inject power at points where sensitive loads are connected during the voltage interruption created by three-phase faults. In this paper, few of important PQ concerns which have been addressed are momentary sags, harmonics, swells, transients and DC offsets, among other important PQ issues. As mentioned, the operation of

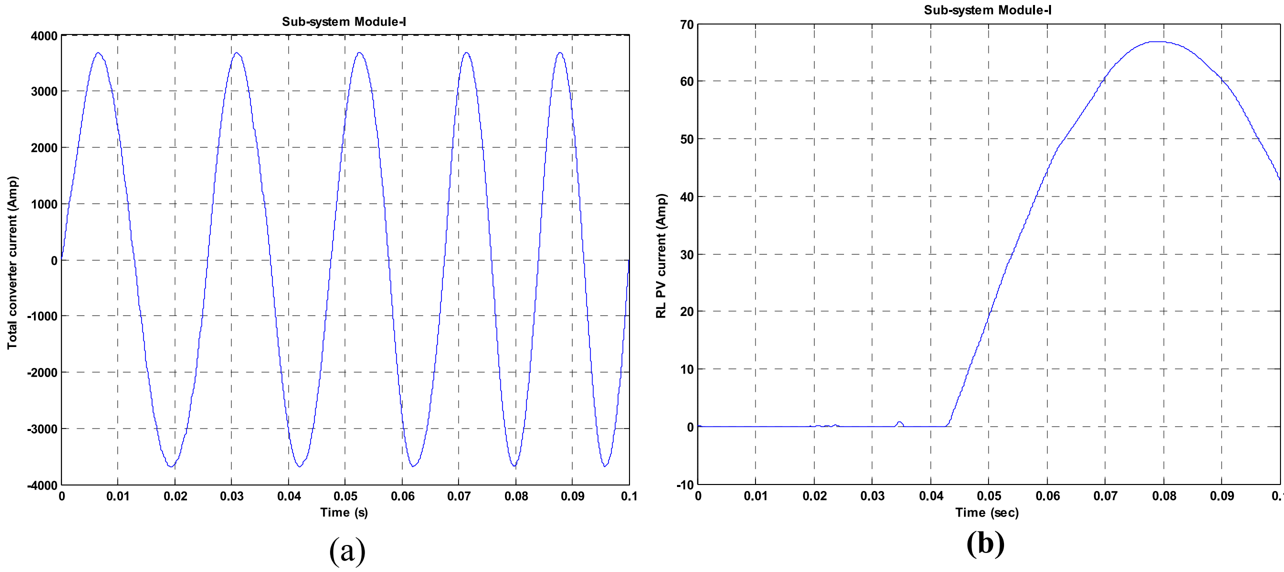

Fig. 4. a) Load current of sub-system module-I b) Current of *RL*-solar PV array.

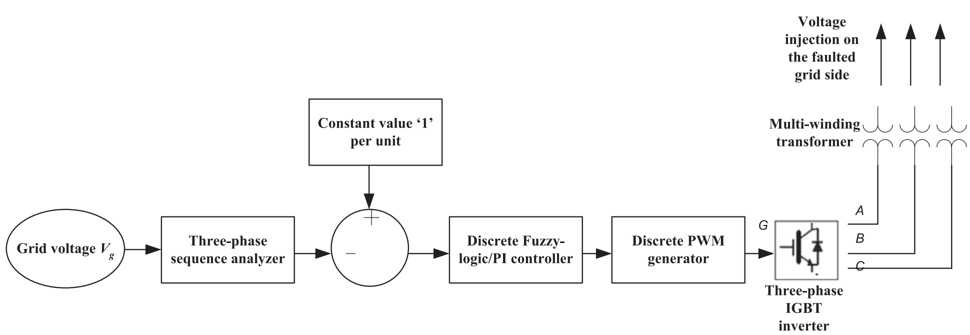

Fig. 5. Schematic of DVR configuration controlled by FLC/PI controller.

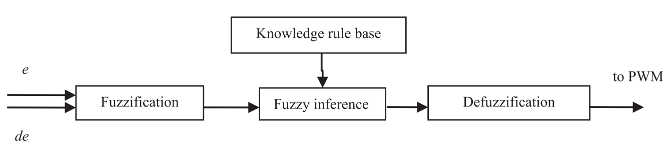

Fig. 6. Block diagram of fuzzy logic controller.

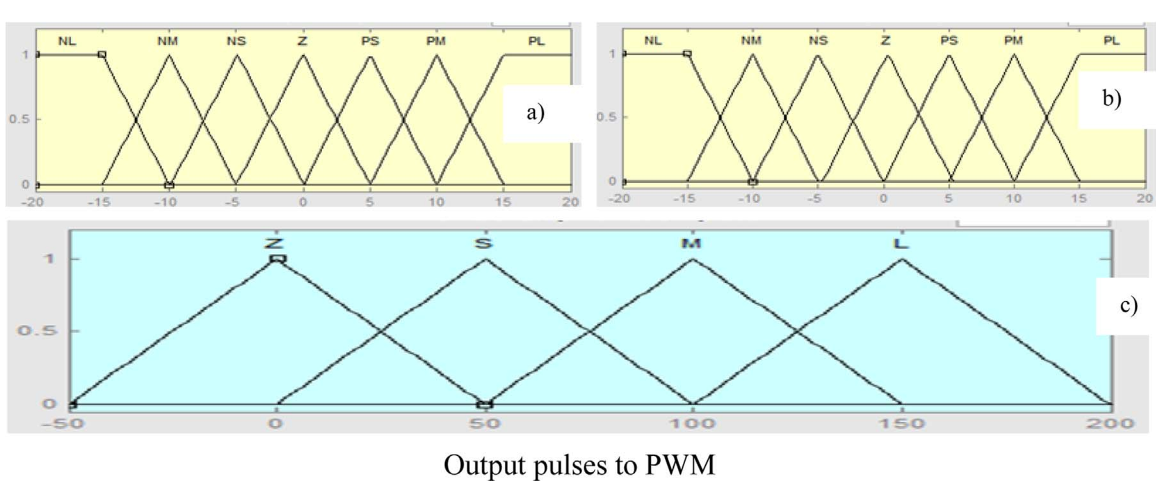

Fig. 7. Membership function of (a) Error *E*, (b) change of error *dE* and (c) output pulse to PWM (defuzzified value).

Table 2
System specifications adopted for three 15-level grid-interactive MMC systems.

System description	Specifications
Sub-system Module-I/II/III	
1. Multi-winding transformer	10 kV, 50 Hz, V_p = 250 V, V_s = 25 V
1. *R-L* load	5 Ω, 0.5 H
1. Thyristor	Snubber resistance = 500 Ω, Snubber capacitance = 250 pF
SPV array	
1. No. of cells in series, N_s	3000
1. No. of cells in parallel, N_p	14
1. Photo-current, I_{ph}	5 A
1. Cell temperature, T_c	20 °C
1. Series resistance, R_s	0.00011 Ω
1. Identity factor, a	1.65
Pulse generator	
1. Amplitude	5
1. Time Period	0.02 s
1. Pulse-width	50%
LCL filter	
1. *LCL*	1500 µH, 30 µF, 1500 µH
Linear *RLC* load	
1. Active power	30 kW
1. Reactive power	10 Kvar
Three-phase programmable voltage source	440 V RMS, unity power factor, 50 Hz
DVR	
1. IGBT inverter	Snubber resistance = 100 kΩ
1. DC voltage source	3.1×10^{6}
1. *LC* filter	V $L = 1\times10^{-3}$ H, C = 750 µF
1. Three winding linear transformer	440 V, 250 MVA, 50 Hz
1. PI controller gain	$K_p = 7$, $K_i = 1050$

DVR is carried out through two different controlling schemes: one is PI and another one is FLC. The accurateness of proposed model is verified by demonstrating the effectiveness of FLC over PI control.

2.1. Simulink behavior of 15-level multilevel converter module

Fifteen-level control strategy: The simulink model for a 15-level converter (Module-I) is depicted in Fig. 2. A multilevel converter circuit with a *RL* component and a DC source works in two modes of operation: one is in rectification mode and another one is in inversion mode [10]. Hence, in order to elaborate the performance of module under changing environmental conditions, the DC source is replaced with a SPV array. The SPV array has been isolated from the utility grid through a multi-winding transformer. The proposed system works in inversion mode only, when the switching angle of each of the converter is greater than 90°. For a 15-level line current, a set of secondary windings with centre-tap arrangement is required. Each pair of thyristor in a centre-tapped secondary winding is fired at a switching delay of 180°. The thyristor at upper leg is fired at an angle greater than 90° for inverter operation. Simultaneously, the thyristor at lower leg is fired with a delay of 180° with respect to the thyristor at upper leg. The phase delays for thyristors proposed in the scheme are summarized in Table 1.

2.2. Solar photovoltaic array modeling

The basic building block of SPV array is a SPV cell [1], which converts incident solar radiation into DC current directly using PV effect. Fig. 3 depicts the electrical equivalent circuit of a SPV cell, which is composed of a light generated current source at input. A single diode is connected in parallel, which represents non-linear impedance of *p-n* junction. On the other hand, the series resistance R_s is the sum of several structural resistances of the SPV device. The value of series resistance is multiplied by number of series-connected SPV cells. The shunt resistance R_p is a loss mainly due to leakage current of *p-n* junction and depends on fabrication method a SPV cell.

The basic mathematical equation for output current is obtained from the theory of semiconductors that describes the *I-V* curve of a SPV cell [44,45] is,

$$I_a = I_{ph}N_p - I_{rs}N_p e^{\{(\frac{q}{akT_c(\frac{V_a}{N_s}+\frac{I_aR_s}{N_p})}-1)\}} - \frac{N_p}{R_p}\left(\frac{V_a}{N_s} + \frac{I_aR_s}{N_p}\right) \tag{1}$$

where:

a: Diode quality factor, I_a: Output current of a single SPV cell (A), I_{ph}: Light-generated current or photocurrent (A), I_{rs}: Reverse saturation current (A), k: Boltzmann's constant (1.38×10^{-23} J K^{-1}), N_p: Number of cells in parallel, N_s: Number of SPV cells in series, q: an electronic charge (1.602×10^{-19} C), R_p: Parallel resistance (Ω), R_s: Series resistance (Ω), T_c: SPV cell's known operating temperature (°K).

The SPV cell output voltage V_a is a function of the photocurrent, which is determined by load current.

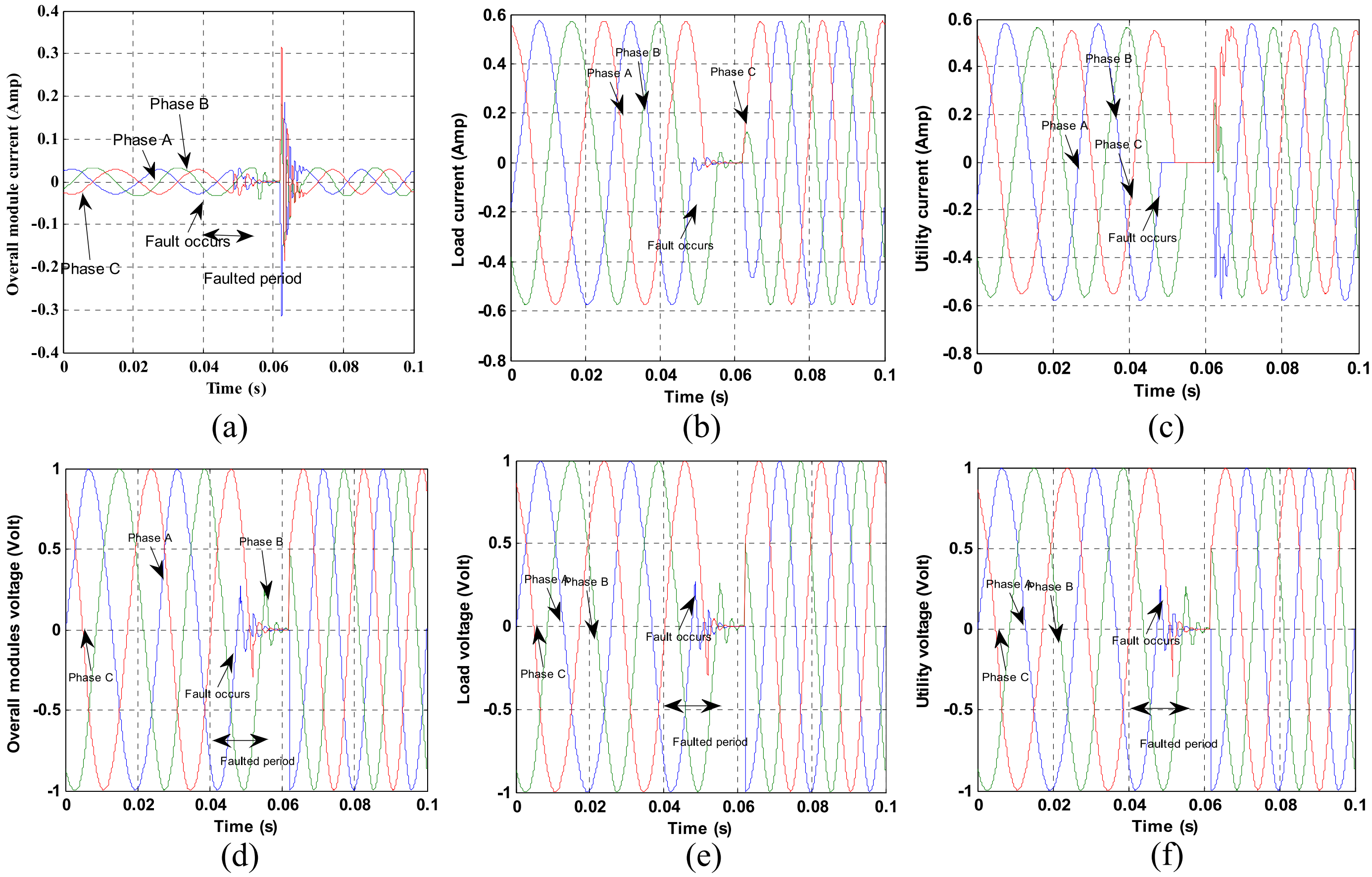

Fig. 8. Under faulted conditions, results of (a-c) module current, load current, and utility current (d-f) module voltage, load voltage, and utility voltage.

$$V_a = \frac{akT_c}{q}\ln\left(\frac{I_{ph} + I_{rs} - I_a}{I_{rs}}\right) - R_s I_a \tag{2}$$

The above equation gives output voltage of a single SPV cell [46]. When it is multiplied by number of cells connected in series, it gives full array output voltage. Thus, if the level of ambient temperature and solar radiation changes, there is a corresponding change in output voltage and current of SPV array. Therefore, in this paper, the effects of ambient temperature and solar radiation levels have been included in final SPV array model. These effects are represented in the model by Eqs. (3)–(4) as:

$$C_{tv} = 1 + \beta_t (T_a - T_x) \tag{3}$$

$$C_{ti} = 1 + \gamma \frac{(T_x - T_a)}{S_c} \tag{4}$$

where, β_t =0.0042 and γ=0.062 for the SPV cell used, and T_a=20 °C, is ambient temperature during the cell testing, C_{tv}: Voltage temperature coefficient (V °C^{-1}), C_{ti}: Current temperature coefficient (A °C^{-1}).

This is used to obtain the modified model of SPV cell for another ambient temperature T_x. A change in solar radiation causes a change in cell photocurrent, and operating temperature, which in turn affects SPV cell output voltage. If solar radiation increases from S_{x1} to S_{x2}, SPV cell operating temperature and photocurrent will also increase from T_{x1} to T_{x2} and from I_{ph1} to I_{ph2}, respectively. Thus change in operating temperature and photocurrent due to variation in solar radiation are expressed as,

$$C_{sv} = 1 + \beta_t \alpha_s (S_x - S_c) \tag{5}$$

$$C_{si} = 1 + \frac{(S_x - S_c)}{S_c} \tag{6}$$

where, C_{sv}: correction factor for change in SPV cell output voltage due to solar radiation, C_{si}: correction factor for change in SPV cell output current due to solar radiation. The constant α_s=0.011 is slope of change in SPV cell operating temperature due to change in solar radiation level. Using Eqs. (3)–(6), the new values of SPV cell output voltage V_{an} and photocurrent I_{phn} at new temperature T_x and solar radiation S_x are obtained as,

$$V_{an} = C_{tv} C_{sv} V_a \tag{7}$$

$$I_{phn} = C_{ti} C_{si} I_{ph} \tag{8}$$

V_a and I_{ph} are benchmark reference SPV cell output voltage and reference cell photocurrent, respectively.

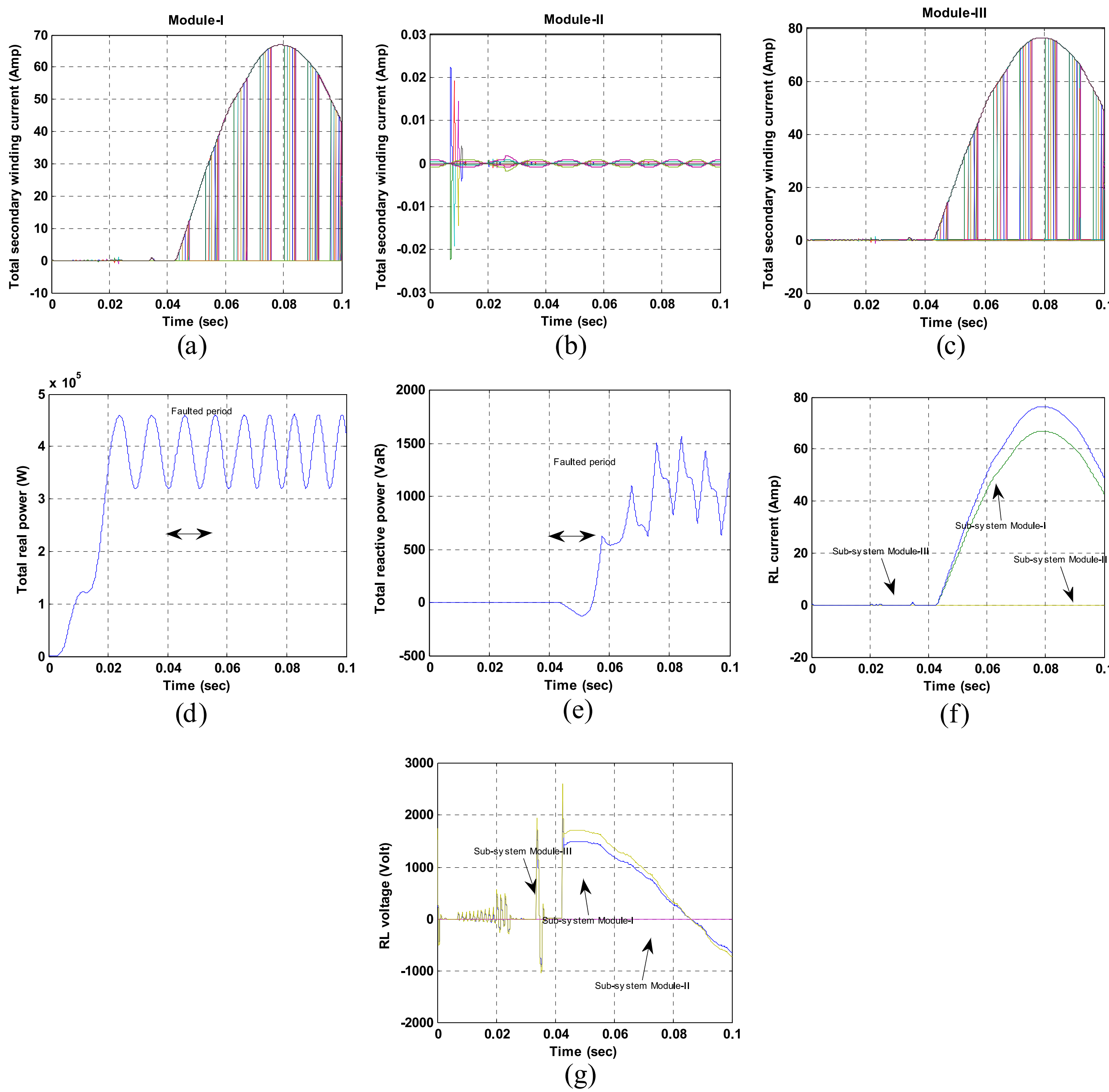

Fig. 9. Under faulted conditions, results of (a-c) secondary winding current of Module-I, II and III (d-e) Real power and reactive power output (f-g) *RL* current and voltage.

3. Control strategy

In general, the load current can be continuous or discontinuous. In the case of continuous current operation the current of both thyristors overlaps. It depends upon DC voltage source, phase angle of load or inductor φ and the switching angle α [10,23]. The expression of the converter current is obtained by solving the equation:

$$L\frac{di}{dt} + iR = V_m \cos \omega t + E \tag{9}$$

For $\omega t = \theta$ and $m = (\frac{E}{Vleg1})$, it gives i_{leg1} for conduction through T_1 in positive half cycle in upper leg of converter.

$$i_{leg1} = \cos(\theta - \varphi) + \frac{m}{\cos(\varphi)} *(1 - e^{\frac{1(\theta-\alpha)}{\tan(\varphi)}}) - \cos(\varphi - \alpha)*e^{\frac{1(\theta-\alpha)}{\tan(\varphi)}} \tag{10}$$

For conduction through T_2 in negative half cycle, the expression of lower leg converter current is given by,

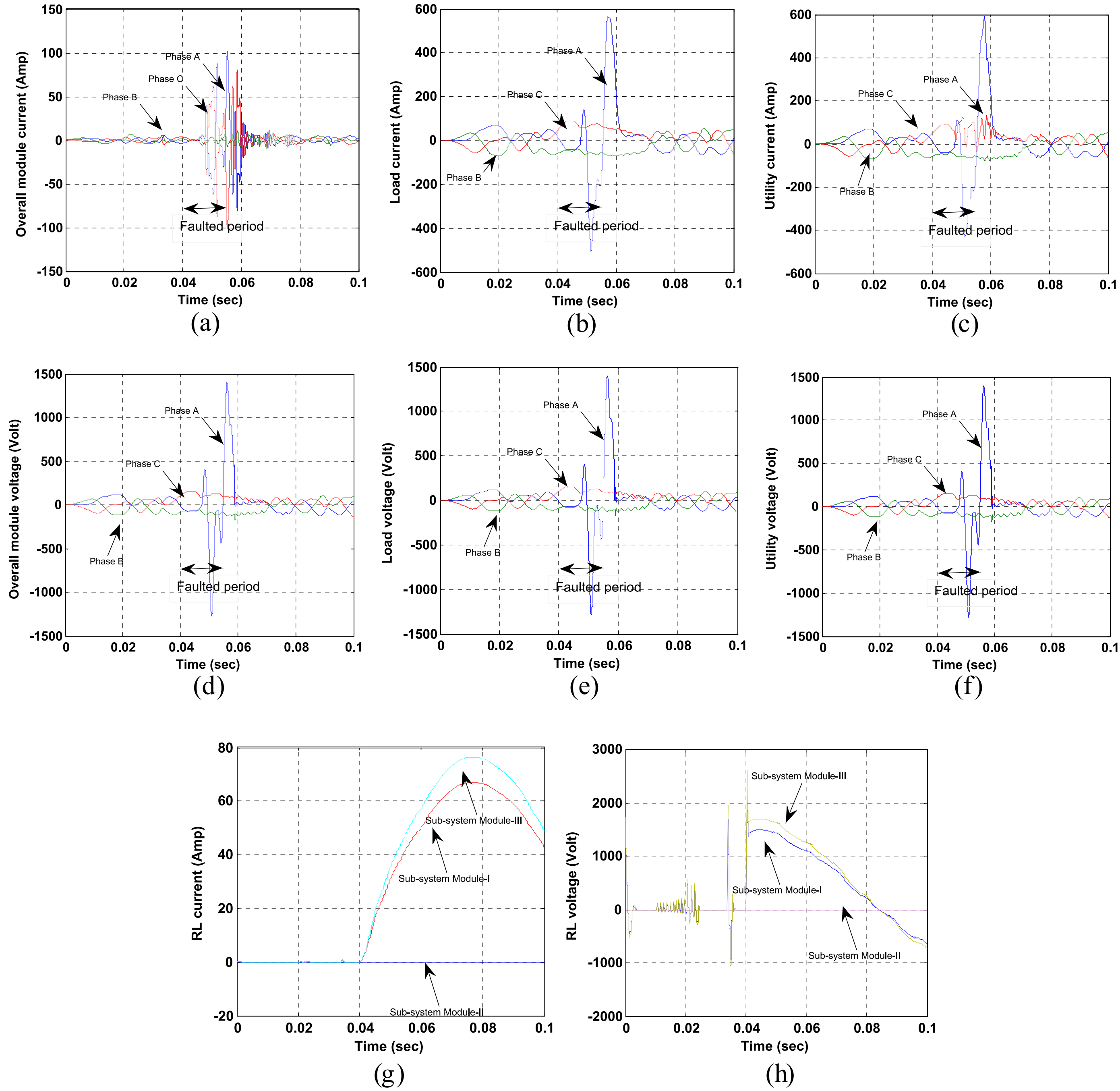

Fig. 10. With PI controlled DVR, results of (a-c) module current, load current, and utility current (d-f) module voltage, load voltage, and utility voltage (g-h) *RL* current and voltage.

$$i_{leg2} = -\cos(\theta-\varphi-\pi) - \frac{m}{\cos(\varphi)}*(1-e^{\frac{1(\theta-\alpha-\pi)}{\tan(\varphi)}}) + \cos(\varphi-\alpha)*e^{\frac{1(\theta-\alpha-\pi)}{\tan(\varphi)}} \tag{11}$$

Each converter contributes to the line current and the net line current i_{line} is equal to sum of currents of both legs (i_{leg1} + i_{leg2}). Thus, the total current of 15-level inverter sub-system module-I is shown through sine waveform in Fig. 4(a). Moreover, the maximum amplitude of the load current is 3.7 kA. In this case, the 15-level converter circuit with *RL* and SPV array load works in the inversion mode, when switching angle of each of the converter is greater than 90°. The DC load side has been isolated from the three-phase utility grid through a multi-winding transformer [47].

3.1. Scheme of dynamic voltage restorer

The general configuration of DVR is depicted in Fig. 5, which consists of a VSC, a harmonic filter, energy storage unit and an injection transformer [48]. The VSC is used to generate the required voltage, which compensates the voltage sag or swells [49,50]. The basic purpose of an energy storage unit is to supply the necessary energy to VSC in order that injected voltage is generated. DVR also mitigates the harmonic content in voltage for any distributed generation system. Apart from this, DVR is also used to remove high frequency components in power. In this paper, the

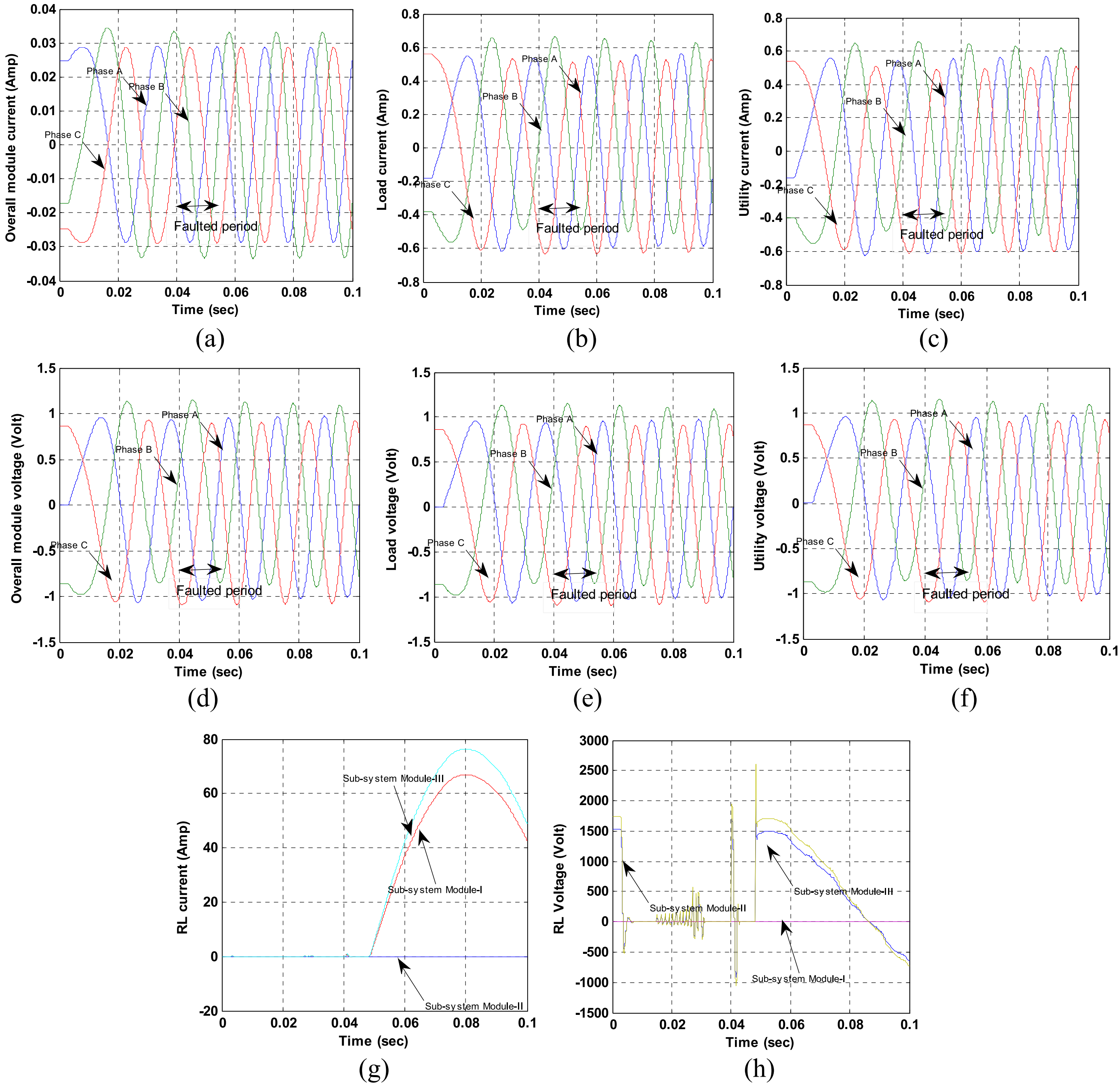

Fig. 11. With FLC-DVR, results of (a-c) module current, load current, and utility current (d-f) module voltage, load voltage, and utility voltage (g-h) *RL* current and voltage.

DVR is implemented for a 15-level MMC with *RL* component and a SPV array as connected load, for three MMC modules.

3.2. Fuzzy-logic controlling scheme for DVR

The DVR control is responsible for controlling the generation of compensating voltage, which is done by controlling the PWM pulses to the gate terminal of VSC [39,51]. To achieve this, fuzzy-logic controller capable of achieving fast compensation is implemented. FLC is preferred over conventional PI controller due to its robustness to system parameter variations during the operation. The fuzzy-logic control scheme exploits the simplicity of the Mamdani type fuzzy systems in design of the controller. As shown in Fig. 6, the fuzzy-logic control scheme can be divided into its four functional sub-systems [9]: knowledge base, fuzzification, inference mechanism and de-fuzzification. In the first stage, the knowledge base consists of data base and rule base. The data base consists of various input-output membership functions, whereas rule base is composed of a set of linguistic rules relating the fuzzy input variables to control actions. In the second stage, the fuzzification converts crisp two input signals: error and change in error, into fuzzy signals, depicted in Fig. 7. In this paper, the grid voltage signal is controlled variable for fuzzy-logic controller. In third stage, the inference mechanism uses the collection of linguistic rules to generate the fuzzy output. Finally, a crisp controlled signal is generated by de-fuzzification which is fed to PWM generator for generating a controlled signal.

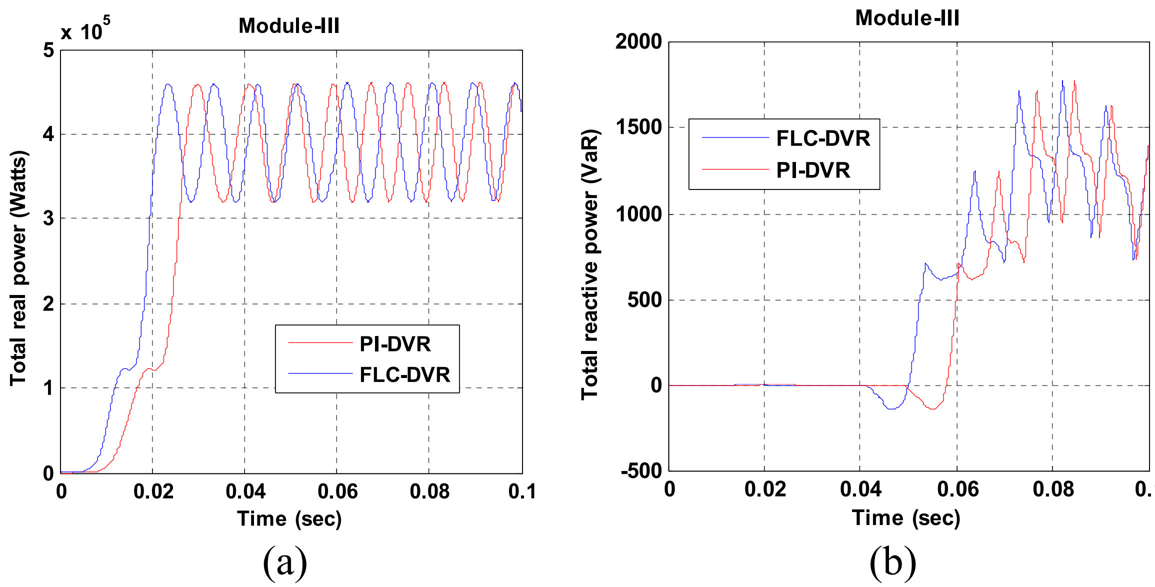

Fig. 12. (a-b) Comparison of PI-DVR and FLC-DVR in real and reactive output power.

Table 3
THD analysis of PI-DVR and FLC-DVR.

	Without any DVR action	PI-DVR	FLC-DVR
Grid side *r* phase	0.2667%	1.203%	0.2657%
Grid side *b* phase	0.2156%	0.9755%	0.2172%
Sub-system Module-I(*PQ*)	2.534%	2.534%	2.534%
Module (s) voltage	0%	28.41%	1.76%
Module (s) current	0%	106.97%	0.21%
Load voltage	0%	28.41%	1.76%
Load current	0%	20.78%	1.98%
Utility voltage	0%	28.41%	1.76%
Utility current	0%	18.88%	1.95%

4. Simulation results and discussion

The simulation of the 15-level MMC system has been performed under the faulted conditions at three-phase grid side. The results for the proposed system are obtained through the Matlab/Simulink model during steady-state and transient conditions. In particular, the total time duration during which the present study is carried out is t=0.1 s. A short-circuited fault at phase C occurs from t=0.040 s to t=0.055 s at PCC of utility grid side. Therefore, the effectiveness of FLC-DVR has been demonstrated during faulted period and results obtained have been compared with PI-DVR for 15-level MMC systems for validation. In addition, the measured values at output of SPV array used in this paper have been experimentally verified [44,45]. MPPT algorithms [52,53] are necessary, because SPV arrays exhibit non-linear voltage-current characteristics with a unique point at which maximum power is produced. Due to this non-linearity of SPV modules, the parameters of SPV module are estimated using particle swarm optimization algorithm in [54]. This proposed algorithm uses time varying acceleration coefficients, which outperforms other conventional algorithms in parameters estimation. In reference papers [55–59], a comprehensive comparison among different types of MPPT techniques is presented and analyzed. The main MPPT techniques have been found to be, perturb & observe or dithering [10], incremental conductance, constant voltage, fuzzy level control neural network, metaheuristic- based MPPT, particle swarm optimization, genetic algorithm, artificial bee colony and ripple correlation factor. A complete analysis on the laboratory implementation of SPV array using a FLC scheme has been done, in order that maximum SPV power is always tracked under stochastically changing levels of temperature and solar radiation. The maximum power points for a SPV array are estimated under ambient temperature and solar radiation levels through a curve-fitted polynomial equation. The specifications of the modules and proposed DVR system are summarized in Table 2.

4.1. Impact of a short-circuit fault on 15-level MMC system

As depicted in Fig. 8(a-f), the transient behavior of total module current in per unit can be observed at t=0.045 s. At t=0.064 s, a sharp transient of 0.3 per unit is evident at PCC due to the presence of a short-circuit fault on utility grid side. The amplitude of overall module current is 0.02 per unit. In this case, there is no flow of load current during the faulted period, however, its per unit value remains constant at 0.58 per unit. Due to the varying level of solar radiation levels being injected into utility, there is a non-uniformity at the maximum amplitude of utility current. This varying nature of current is sum of currents generated by three solar SPV arrays connected in *RLE* loads at the output of three modules. Also, the transients in per unit load current can be observed at t=0.048 s, which makes the load current to attain zero level at t=0.06 s. The effect of a three-phase fault is evident on the utility grid side, when current in per unit attains zero level from t=0.048 s to t=0.06 s. As depicted in Fig. 8(d-f), the effect of a three-phase fault at phase C can also be observed by the presence of a sharp transient at t=0.048 s in over module voltage, load voltage and utility grid voltage.

Fig. 9(a-c) depicts the nature of output current for each module at the secondary of a multi-winding transformer under faulted grid conditions. The total current per module resembles a sinusoidal wave with reduced level of harmonic content. This current remains zero level till t=0.044 s, due to gradual increase of solar radiation level. However, the amplitude of module current rises at t=0.044 s from 0 level to 68 A and 78 A at t=0.08 s, for Module-I and Module-III, respectively. For Module-II, the current has been expressed on per unit basis indicating the presence of sharp transient at t=0.01 s. Corresponding to each of these currents at t=0.044 s, the current behavior of *RL* load for each module corresponds to the envelope of current waveforms. Further, it can be seen that the maximum level of real output power per module is around 4.6×10^5 W at t=0.024 s. This level remains constant till t=0.1 s, which indicates that the real output power of MMC Module-I remains constant even as the level of SPV radiation changes. The real power is maintained constant by varying the switching angle scheme as mentioned in Table 1. Thus for three modules, the total real output power generated will be around 13.8×10^5 W. The response of reactive power per module is negative during the faulted period at t=0.05 s, the amplitude of which rises to 1500 VAR at t=0.084 s. The transient behavior of *RL* voltage can be observed due to switching of each of thyristor at different switching angles.

4.2. Impact of Proportional-Integral controlled DVR on faulted grid side

In this section, the analysis on the impact of PI controlled DVR under the faulted conditions has been presented. The analysis as depicted through Fig. 10 (a-h) includes the impact of SPV array used as part of load during the conversion of DC power into AC power. The conventional PI controller is used in DVR system so that it can inject the voltage at utility-grid side. The nature of overall module current is distorted in nature whereas, the transients are observed during the presence of a short-circuit fault. The impact of fault at phase C has resulted the overall non-uniform module currents during the entire time period of study. The load current is negative, till the time the function of DVR starts. At t=0.042 s, the amplitude of load current becomes around 90 A. A sharp transient in load current at phase A is also evident at t=0.054 s. However, during the presence of a short-circuit fault, the overall load current is positive. It can be noted that a negative transient in grid injected current has been observed, which becomes zero on the fault clearance at t=0.055 s. The removal of short circuit transients is also visible in the waveforms of overall module voltage, load voltage and utility voltage. Except, after the faulted period at t=0.055 s, the transient nature can effectively be controlled by increasing the forward path gain of PI controller. Further, the *RL* current and voltage are controlled by the controller at t=0.040 s, instead of t=0.042 s.

4.3. Impact of Fuzzy-logic controlled DVR on faulted grid side

To further investigate the accuracy of proposed system, the results obtained in Section 4.2. are compared by implementing DVR-FLC. Besides, this study reveals the effective implementation of Mamdani type fuzzy system. The three-phase faulty grid voltage and current are controlled though FLC-DVR, among other controlled variables under faulty conditions as depicted in Fig. 11. The nature of overall module current, load current and utility current becomes sinusoidal during t=0.040 s to t=0.055 s. With FLC-DVR connected in series, the compensating voltage is injected through the transformer, which effectively mitigates the sag and swell in voltage at all levels [60]. Clearly, this action thus maintains voltage level at around 1.00 pu. It is evident that amplitude of *RL* voltage of sub-system Module-II has been increased to 2600 V at t=0.046 s whereas, that of amplitude of *RL* voltage of sub-system Module III has been increased to 1500 V at t=0.046 s.

4.4. Comparative analysis of output power and THD on faulted grid side

In this sub-section, the real output power of FLC-DVR is compared with PI controlled DVR for Module-III. Fig. 12 reveals that the maximum power of module at around 460 kW is generated at t=0.024 s. However, on close observation, it is found that the same power is generated by Module-III at t=0.028 s, while implementing PI controlled DVR. Similarly, the compensation done by generating the reactive power requirement of *RLC* load is achieved with high speed and accuracy by using FLC-DVR as compared to PI-DVR. Using FLC-DVR, the maximum value of compensation achieved is 170 kVAR at t=0.081 s. Clearly, the combined operation of FLC-DVR is rapid as compared to PI-DVR. Table 3 summarizes the THD comparison of PI-DVR and FLC-DVR, where it is evident that FLC is able to reduce the level of harmonic content for module voltage and current at PCC. Standard IEEE-519/1547 stipulates that current injected into the utility by any of distributed generation sources should be less than 5%. As can be seen, the THD of utility injected current is 1.95% using FLC-DVR at unity power factor. Similarly, the THD levels of load voltage and current is found to be less than 5%.

5. Conclusion

This paper has investigated and addressed the important PQ concerns by implementing a DVR into three 15-level MMC systems. It has been revealed that the coordination of proposed system with FLC-DVR has been capable to mitigate the sags and swells rapidly during the faulted conditions at grid side. A thorough analysis has been carried under changing solar radiation and ambient temperature levels, when a hardware validated SPV array has been connected as load with *RL* circuit for each of 15-level MMC module. One of the key objective of reactive power compensation has been achieved. In addition, a comparative analysis on harmonic study has been summarized using PI-DVR and FLC-DVR, which is validated by IEEE-519/1547 standard. FLC-DVR scheme reduces the running time, and ensures the accuracy and quality of derived waveforms at the output. This scheme was found superior to conventioned PI-DVR technique. Fuzzy logic technique proved its effectiveness in PQ measurement under changing environmental conditions, where THD had been taken as a major performance index to examine the effectiveness of the solution. IEEE-519/1547 standard has been an effective tool to prove level of THD cannot be more than 5% for load current and grid injected current at PCC. Overall, the contribution of custom power device like DVR and its integration with SPV connected MMC systems is satisfactory.

5.1. Future work

Hardware implementation of proposed configuration for 15-level three modules of MMC system with a SPV array for the analysis of PQ. A basic prototype for a SPV integrated grid-interactive MMC system can be developed with a basic MPPT controller. An efficient low cost PI and FLC controller can be used for DVR operation and realized for PQ control, especially for faulted conditions at grid or load side.

References

[1] Buresch M. Photovoltaic energy systems design and installation. New York: McGraw-Hill; 1983.
[2] Solanki CS. Solar photovoltaics-fundamentals, technologies and applications, 2nd ed. New Delhi: PHI Learning; 2011, (July).
[3] Khajehoddin AA, Bakhshai A, Jain P. The application of the cascaded multilevel converters in grid connected photovoltaic systems. in: Proceedings of IEEE Electrical Power Conference. Canada, 296-301; 2007.
[4] Blaabjerg F, Teodorescu R, Liserre M, Timbus AV. Overview of control and grid synchronization for distributed power generation. IEEE Trans Ind Electron 2006;53(5):1398–409.
[5] Sahoo SK. Renewable and sustainable energy reviews solar photovoltaic energy progress in India: a review. Renew Sustain Energy Rev 2016;59:927–39.
[6] Mahela OP, Shaik AG. Comprehensive overview of grid interfaced solar photovoltaic systems. Renew Sustain Energy Rev 2017;68:316–32.
[7] Tareena WU, Mekhilefa S, Seyedmahmoudianb M, Horanb B. Active power filter (APF) for mitigation of power quality issues in grid integration of wind and photovoltaic energy conversion system. Renew Sustain Energy Rev 2017;70:635–55.
[8] Rashid MH. Power electronics: circuits, devices and applications, 3rd ed. USA: Academic Press; 2003.
[9] Bose BK. Modern power electronics and ac drives. USA: Prentice-hall; 2002.
[10] Mohan N, Undeland TM, Robbins WP. Power electronics: converters, applications and design [September]. Wiley; 2003.
[11] Kumar J, Das B, Pramod A. Selective harmonic elimination technique for a multilevel inverter. in: Proceedings of 15th National Power Systems Conference (NPSC), Bombay; December, 608-613; 2008.
[12] Lai JS, Peng FZ. Multilevel converters-a new breed of power converters. IEEE Trans Ind Appl 1996;32(3):509–17.
[13] Tolbert LM, Chiasson JN, Du Z, Mckenzie KJ. Elimination of harmonics in a multilevel converter with nonequal DC sources. IEEE Trans Ind Appl 2005;41(1):75–81.
[14] Tolbert LM, Peng FZ, Habetler TG. Multilevel converters for large electric drives. IEEE Trans Ind Appl 1999;35(1):36–44.
[15] Adam GP, Anaya O, Burt G, Telford D, Williams B, Mcdonald J. Modular multilevel inverter: pulse width modulation and capacitor balancing technique. IET Power Electron 2010;3:702–15.
[16] Rajasekar S, Gupta R. Solar photovoltaic power conversion using modular multilevel converter. in: Proceedings of IEEE Conference on Engineering and systems, India; March, 1-6; 2012.
[17] Razvani A, Gandomkar M. Modeling and control of grid connected intelligent hybrid photovoltaic system using new hybrid fuzzy-neural method. Sol Energy 2016;127:1–18.
[18] Letting LK, Munda JL, Hamam Y. Optimization of a fuzzy logic controller for PV grid inverter control using S-function based PSO. Sol Energy 2012;86(6):1689–700.
[19] Benner JP, Kazmerski L. Photovoltaics gaining greater visibility [September]. IEEE Spectr 1999;29(9):34–42.
[20] Messenger RA, Ventre J. Photovoltaic systems engineering. New York: CRC Press; 2004.
[21] Rauschenbach HS. Solar cell array design handbook-the principles and technology of photovoltaic energy conversion. New York: Van Nostrand Reinhold; 1980.
[22] Suresh Y, Panda AK. Investigation on hybrid cascaded multilevel inverter with reduced DC sources. Renew Sustain Energy Rev 2013;26:46–59.
[23] Sarwar A, Asghar MSJ. Multilevel converter topology for solar PV based grid-tie inverters. in: Proceedings of IEEE conference on energy conference and exhibition, Manama; December, 501-506; 2010.
[24] Sarwar A, Asghar MSJ. Simulation and analysis oa a multilevel converter topology for solar PV based grid connected inverter. Smart Grid Renew Energy 2011;2:56–62.
[25] Latran MB, Teke A. Investigation of multilevel multifunctional grid connected inverter topologies and control strategies used in photovoltaic systems. Renew Sustain Energy Rev 2015;42:361–76.
[26] Calais M, Agelidis GA, Meinhardt M. Multilevel converters for single-phase grid connected photovoltaic systems: an overview. Sol Energy 1999;6(5):325–35.
[27] Rahim NA, Selvaraj J, Krismadinata C. Five level inverter with dual reference modulation technique for grid-connected PV system. Renew Energy 2010;35(3):712–20.
[28] Ravi A, Manoharan PS, Anand JV. Modeling and simulation of three phase multilevel inverter for grid connected photovoltaic systems. Sol Energy 2011;85(11):2811–8.
[29] Bandara K, Sweet T, Ekanayake J. Photovoltaic applications for off-grid electrification using novel multi-level inverter technology with energy storage. Renew Energy 2012;37(1):82–8.
[30] Kang FS, Cho SE, Park SJ, Kim CU, Ise T. A new control scheme of a cascaded transformer type multilevel PWM inverter for a residential photovoltaic power conditioning system. Sol Energy 2005;78(6):727–38.
[31] Kaliamoorthy M, Rajasekran V, Raj IGC. Single-phase fifteen level grid-connected inverter for photovoltaic system with evolutionary programming based MPPT algorithm. Sol Energy 2014;105:314–29.
[32] Al-Othman AK, Abdelhamid TH. Elimination of harmonics in multilevel inverters with non-equal dc sources using PSO. Energy Convers Manag 2009;50:756–64.
[33] Himour K, Ghedamsi K, Berkouk EM. Supervision and control of grid connected PV-Storage systems with the five level diode clamped inverter. Energy Conv Manag 2014;77:98–107.
[34] Prabaharan N, Palanisamy K. Analysis and integration of multilevel inverter configuration with boost converters in a photovoltaic system. Energy Convers Manag 2016;128:327–42.
[35] Altin N, Ozdemir S. Three-phase three-level grid interactive inverter with fuzzy logic based maximum power point tracking controller. Energy Convers Manag 2013;69:17–26.
[36] Kakosimos P, Pavlou K, Kladas A, Manias S. A single-phase nine-level inverter for renewable energy systems employing model predictive control. Energy Convers Manag 2015;89:427–37.
[37] Hingorani NG. Introducing custom power [June]. IEEE Spectr 1995;32(6):41–8.
[38] Sankaran C. Power Quality. USA: CRC Press; 2002.
[39] Chakraborty A. Advancements in power electronics and drives in interface with growing renewable energy resources. Renew Sustain Energy Rev 2011;15:1816–27.
[40] Shivashankar S, Mekhilef , Mokhlis H, Karimi M. Mitigating methods of power fluctuation of photovoltaic (PV) sources-a review. Renew Sustain Energy Rev 2016;59:1170–84.
[41] Albert AS. Development of solar photovoltaic inverter with reduced harmonic distortions suitable for Indian sub-continent. Renew Sustain Energy Rev 2016;56:694–704.
[42] Matlab/Simulink, The Mathworks, Inc., 7.10.0.499 (R2010a), Available: ⟨http://www.mathworks.com⟩.
[43] IEEE-519/1547. IEEE standard for interconnecting distributed resources with electric power systems. 2003.
[44] Altas IH, Sharaf AM. A fuzzy logic power tracking controller for a photovoltaic energy conversion scheme. Electr Power Syst Res 1992;25:227–38.
[45] Altas IH, Sharaf AMA. PV array simulation model for Matlab-Simulink GUI environment. in: Proceedings of International Conference on Clean Electrical Power Capri (ICCEP), 341-345; 2007.
[46] Jordehi AR. Parameter estimation of solar photovoltaic (PV) cells: a review. Renew Sustain Energy Rev 2016;61:354–71.
[47] Gonzalez M, Cardenas V, Miranda H, Ricardo AS. Conception of a modular multilevel converter for high-scale photovoltaic generation based on efficiency criteria. Sol Energy 2016;125:381–97.
[48] Ramasamy M, Thangavel S. Experimental verification of PV dynamic voltage restorer (PV-DVR) with significant energy conservation. Int J Electr Power Energy Syst 2013;49(7):296–307.
[49] Chung IIY, Won DJ, Park SY, Moon SII, Park JK. The DC link energy control method in dynamic voltage restorer system. Int J Electr Power Energy Syst 2003;25(7):525–31.
[50] Banaei MR, Hosseini SH, Khanmohamadi S, Gharehpetian GB. Verification of a new energy control strategy for dynamic voltage restorer by simulation. Int J Simul Model Pract Theory 2006;14(2):112–25.
[51] Holtz J. Pulse width modulation-a survey. IEEE Trans Ind Electron 1992;39(5):410–20.
[52] Dileep G, Singh SN. Maximum power point tracking of solar photovoltaic system using modified perturbation and observation method. Renew Sustain Energy Rev 2015;50:109–29.
[53] Gomathy S, Saravanan S, Thangavel S. Design and implementation of maximum power point tracking (MPPT) algorithm for a standalone PV system. Int J Sci Eng Res 2012;3(2):1–7.
[54] Jordehi AR. Time varying acceleration coefficients particle swarm optimisation (TVACPSO): a new optimisation algorithm for estimating parameters of PV cells and modules. Energy Convers Manag 2016;129:262–74.
[55] Esram T, Chapman PL. Comparison of PV array maximum power point tracking techniques. IEEE Trans Energy Convers 2007;22(2):443–9.
[56] Ansari MF, Iqbal A, Chatterji S. A fuzzy logic control scheme for a solar photovoltaic system for a maximum power point tracker. Int J Sustain Energy 2010;29(5):245–55.
[57] Coelho RF, Concer FM, Martins DC. A MPPT approach based on temperature measurements applied in PV systems. in: Proceedings of 9th International Conference On Industry Applications (INDUSCON), IEEE, Sao Paulo; November, 1-6; 2010.
[58] Molina MG, Juanico LE. Dynamic modeling and control design of advanced PV solar System for distributed generation applications. J Electr Eng: Theory Appl 2010;1(3):141–50.
[59] Jordehi AR. Maximum power point tracking in photovoltaic (PV) systems: a review of different approaches. Renew Sustain Energy Rev 2016;65:1127–38.
[60] Bollen MHJ. Understanding power quality problems: voltage sags and interruptions. New York: IEEE Press; 2000.

Associate Professor
Akhil Gupta
Department of Electrical Engineering, University Institute of Engineering, Chandigarh University, Chandigarh-Ludhiana highway, Mohali, 140413 Punjab, India
E-mail address: akhilgupta1977@gmail.com